International Journal of Thermofluids 3–4 (2020) 100026

Contents lists available at ScienceDirect

International Journal of Thermofluids

journal homepage: www.elsevier.com/locate/ijtf

Diesel/syngas co-combustion in a swirl-stabilised gas turbine combustor

Ogbonnaya Agwu*, Agustin Valera-Medina

School of Engineering, Cardiff University, CF24 3AA, Cardiff, UK

ARTICLE INFO

Article History:
Received 19 February 2020
Revised 10 March 2020
Accepted 11 March 2020
Available online 17 March 2020

Keywords:
Dual fuel
Combustion
Emissions
Flame stability

ABSTRACT

Multiphase fuel combustion was carried out in a swirl-stabilised combustor with the aim of expanding the fuel flexibility of the gas turbine for, at least, land-based applications. Improved capability of the gas turbine in this regard will not only augur well for energy security but also could be useful in tackling harmful emissions. In the study, varying amounts of syngas was premixed with air and swirled into a burning diesel spray, the flowrate of which was altered to maintain the same overall heat output at all times. Across the several heat outputs tested, the range of stable flame operation was found to reduce as gas content of fuel mix increased. Moreover, for a combined heat output of 15 kW and a global equivalence ratio of 0.7, a steady increase in flame stability was noted and NO_X emissions were found to decrease while CO emissions increased as syngas content in fuel mix increased from 10% to 30%. The increase in flame stability, achieved at the cost of lower heat release rate, was attributed to the changes in reacting flow dynamics evinced by the C_2^* and CH^* species chemiluminescence intensity variation as well as chemical kinetics analysis. The NO_X and CO emissions trend was ascribed to decreasing combustion efficiency due to poorer spray quality obtained from the pressure atomiser as liquid flow rate reduces and further worsened by the lower heat release rate and decreasing adiabatic flame temperature as gas ratio of combusted fuel increases.

1. Introduction

Research into multiphase fuel combustion in internal combustion (IC) engines where a carbon-rich fuel like diesel is partially replaced by low-carbon fuels like natural gas is gaining traction not only because of the need to cater to environmental concerns but also the improved fuel flexibility of the IC engine bodes well for energy security. Commonly, multiphase combustion tests are carried out in diesel engines by 'fumigating' the intake air with gaseous fuel then igniting the premixed charge with diesel spray [1]. As well as typical diesel engine performance parameters (brake torque, thermal efficiency, specific fuel consumption etc), post combustion emissions – notably NO_X, CO and CO_2 – from the dual fuel tests are measured and compared with conventional diesel engine operation [2-4]. Whereas there exists some disparity regarding the impact of dual fuel burn on diesel engine performance, understandable because of the considerable variation in materials, equipment and methods amongst published studies, there is no doubt about the feasibility of the co-combustion process. This is evident from the extensive range of fuel combinations trialled including diesel/natural gas [5], diesel/hydrogen [6,7], diesel/biogas [8], biodiesel/biogas [9], primary alcohols/natural gas [10].

However, the scope of dual fuel burn in continuous combustion engines like the gas turbine is limited. The focus has been on co-combustion of blends of fuels in the same phase like the liquid phase fuel combinations in [11–15] and the gaseous ones in [16–22]. Multiphase fuel combustion experiments in gas turbine conditions are rarer. Flame structure and local extinction characteristics of ethanol/methane co-combustion in a swirl-stabilised gas turbine combustor was studied by Sidey and Mastorakos [23] providing some fundamental understanding of dual-fuel combustion in continuous flow devices. Subsequently, replacing ethanol with a non-oxygenated liquid fuel – *n*-heptane – but still utilising CH_4 as the gaseous fuel, Sidey and Mastorakos [24] showed how spray flame behaviour and stabilisation characteristics are altered as a consequence of multiphase combustion in the same burner. Additional characterisation of the swirling dual fuel flame of [24] in the form of temperature and reaction zone imaging was provided in Evans et al. [25]. Further, at high (600 K) combustion air inlet temperature, [26] investigated biodiesel co-combustion with natural gas in a radial swirl burner at low equivalence ratios comparing the emissions results with equivalent natural gas and kerosene co-combustion. The characteristics of palm biodiesel and natural gas co-firing in a model swirl flame burner with a combustion inlet air temperature of 523 K was investigated by [27] and compared with neat biodiesel combustion in terms of OH^* and CH^* radical intensity as well as post combustion emissions.

* Corresponding author.
E-mail address: AgwuOE@cardiff.ac.uk (O. Agwu).

https://doi.org/10.1016/j.ijft.2020.100026

Like in the diesel engine studies, the goal of these experiments in simultaneous combustion of different fuels is to combat environmental pollution and, by expanding the fuel flexibility of the engines, tackle the problem of energy security. To more realistically move towards this goal of improved fuel flexibility in the context of multiphase combustion for the gas turbine, practical fuels needs to be employed in the experiments. It is to this end that the present study trialled diesel and syngas co-combustion in a swirl-stabilised gas turbine burner. Syngas is an alternative fuel that has been satisfactorily employed in gas turbine combustion studies such as [19,20,28]. It is generally composed of H_2, CO, CO_2, CH_4, N_2 and steam; the presence and concentration of each constituent depending on the feedstock and synthesizing technique employed. The inert nature of N_2 and the diluting effects of CO_2 and steam diminishes, oftentimes significantly, the heating value of syngas compared to natural gas. The reduction in heating value causes an increase in volume of syngas combusted if similar power output is to be achieved. Combustor chamber modification will then be required in order to accommodate this increased fuel volume resulting in a perturbing of combustion zone properties and associated operational issues like blowout and flashback [28]. Therefore, in order to avoid wholesale changes to a burner setup previously tested with methane and diesel co-combustion [29], a syngas mixture of 10% H_2, 10% CO and 80% CH_4 – having comparable adiabatic flame temperature, laminar flame speed and volumetric heat release rate as CH_4 – was used in the present study. Increasing amounts of syngas was premixed with combustion air then passed through a swirler and into a burning diesel spray. With overall power output held constant, C_2^* and CH^* chemiluminescence imaging as well as post combustion emissions measurement were carried out for three different multiphase cases at the same power output and equivalence ratio. The results were compared with neat diesel combustion with chemical kinetics studies adding to the analysis. Also, the stable flame operating range for different combinations of the two fuels were established and contrasted with the range obtainable for neat diesel combustion in the burner.

As noted previously, studies on multiphase fuel combustion in gas turbine engines are limited and tests utilising the fuel combination in this study, as far as the authors know, is non-existent in published literature. Consequently, this study fills that gap and provides data pertaining to multiphase fuel combustion dynamics, stability and extinction issues in swirl-stabilised gas turbine combustors. Apart from the potential of utilising multiphase fuels in staged combustion, at least one OEM, at present, have combustion turbines with dual fuel capability allowing for continuous operation even as fuels are switched with plans for further expansion [30]

2. Method

2.1. Experimental setup

Diesel spray via a Delavan 0.4 GPH 60^0W pressure nozzle was combusted in air premixed with syngas. The diesel flow rate across the nozzle was controlled by means of a Bronkhorst mini Cori-flow mass flow controller (MFC) having an accuracy of ±0.2% of indicated reading. Diesel supply to the MFC was achieved using a Walbro GSL 392 inline fuel pump delivering the fuel at a constant pressure of 0.85 MPa measured upstream of the MFC. Combustion air was metered by means of two variable area flowmeters. One was of range 30 – 150 l/min with an accuracy of ±1.25% and the second had a range between 40 – 440 l/min with an accuracy of ±5%. Air flow was split between the two meters to avoid operating close to the limits of the device thereby minimising associated errors. Syngas flow rate was controlled by means of a Bronkhorst El-flow Prestige MFC with a rated accuracy of ±0.5%. As earlier mentioned, the gases – combustion air and syngas – were premixed prior to combustion by introducing them simultaneously into the burner inlet air plenum. The charge undergoes further mixing as it passes through the swirler (see Fig. 1).

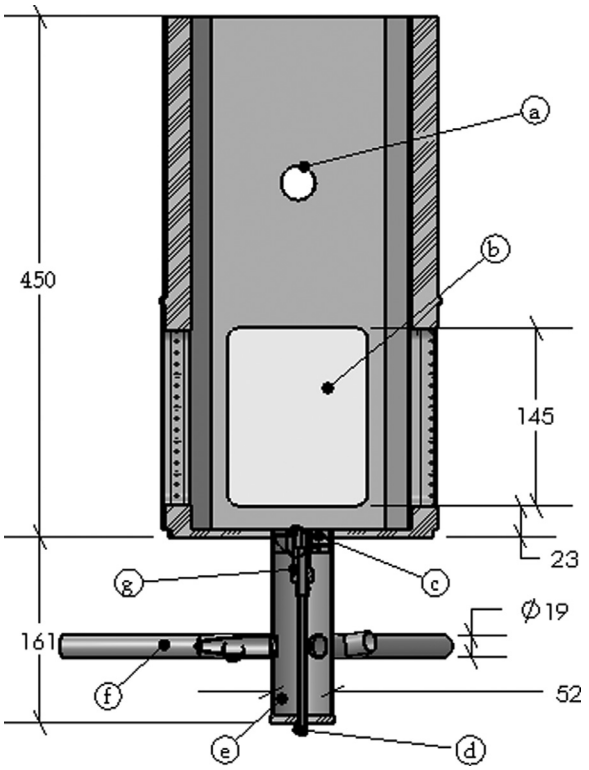

Fig. 1. Burner configuration for diesel/syngas co-combustion. (a) emissions probe slot (b) quartz window (c) axial swirler (d) liquid fuel line (e) inlet plenum (f) combustion air/gas fuel inlet (g) pressure atomiser. All dimensions in millimetres.

The swirler sits flush with the nozzle orifice plane and has five swirl vanes, a tip diameter of 50 mm and a hub diameter of 16 mm. The geometric swirl number is calculated from Eq. (1) to be 1.24. In Eq. (1), D_s refers to the tip diameter while D_h is the hub diameter and θ, the angle of swirl, is 60^0. The combustion chamber has a square cross section of side 180 mm and height 450 mm. Quartz windows on each side of dimension 100 × 145 mm allows multiple optical access albeit the base of each window is 23 mm from the dump plane of the burner.

$$S_N = \frac{2}{3}\left[\frac{1-(D_h/D_s)^3}{1-(D_h/D_s)^2}\right]\tan\theta \quad (1)$$

2.2. Emissions acquisition

Two forms of emissions were of interest in the study – optical emissions from two intermediate combustion species (C_2^* and CH^*) as well as pollutant emissions, namely NO_X and CO. The setup to capture optical emissions included an LaVision CCD Imager Intense camera, a high speed IRO intensifier and a 60 mm focal length AF Micro-Nikkor (f/2.8) lens coupled to each other in the order listed and directed towards the centreline of the burner. The focus was on a plane ±50 mm in the radial direction and 140 mm in the axial direction resulting in a resolution of 0.124 mm/pixel. Chemiluminescence emissions of C_2^* and CH^* species were acquired by fitting bandpass filters centred at 515 nm and 430 nm respectively at the end of the lens; each filter had a full width at half maximum (FWHM) of 10 nm. The species targeted - C_2^* and CH^* - were selected because, not only are they good indicators of heat release rate in hydrocarbon flames but also their emission spectra are prominent in liquid fuelled combustors with clearly identifiable peaks at the selected bandwidths [31-35]. With optimal intensifier settings determined by preliminary studies, 250 chemiluminescence images at 10 Hz were captured for each test point per species. The images were then temporally

averaged and background corrected. Finally, to obtain the images presented in Section 3.2, Abel inversion was carried out on the averaged and background corrected image by adapting the Matlab code used and described by Runyon et al. [36].

The post combustion emission measurements of NO_X and CO were done using Testo 350 XL emissions analyser with the emissions probe situated at the centreline of the burner, 300 mm from the nozzle orifice plane. The emissions analyser was programmed to sample flue gas for a duration of two minutes at a measuring rate of three seconds for each test condition resulting in a total of forty readings per experimental run. Reported NO_X measurements are made on a dry basis. The Testo draws the flue gas through the probe into the gas preparation unit where it is suddenly cooled to 4 – 8°C precipitating condensation. The dry gas is subsequently filtered and passed to the gas sensors which then issue a signal. It was noted that both emissions readings stabilised well before the last twenty readings; the average of the last twenty readings is reported in this work. A rinse time of five minutes followed the completion of each programmed run of the device prior to commencement of a new run. For the emissions reported, the equipment has a measurement uncertainty of ±5 %. The oxygen reference was set at 15% for the tests.

2.3. Fuels and operating conditions

In Table 1 are physical and chemical properties of the fuels tested whereas in Table 2, the fuel/air combinations of the four different test cases and the bulk swirling gas velocities for each are presented. The diesel used in the study is of the BS EN590 standard. The syngas composition was 10% hydrogen, 10% carbon monoxide and 80% methane. Based on mole fraction composition, the density, lower heating value and stoichiometric fuel/air ratio for the syngas shown in Table 1 were determined. The liquid/gas ratio of combusted fuel was altered based on energy share ratio from 100/0 to 70/30. A 90/10 liquid/gas ratio (LGR), for example, implying that 90% of the total heat output is supplied by the diesel and 10% by syngas.

This method of splitting combusted fuels in multiphase burning was used in [7,8,10] and advantageous for this study because it means a fairly constant air flow rate for all test conditions (Table 2) being that both fuels have similar heating values. Consequently, cold flow characteristics are more or less maintained across the different test cases. Furthermore, given that a pressure atomiser was employed for diesel injection and that the pressure upstream of the MFC was maintained, trials conducted at flow rates corresponding to liquid/gas ratios below 70/30 were of very poor spray quality thereby adversely affecting combustion efficiency. Consequently, the chemiluminescence and emissions tests were limited to the LGR range given in Table 2.

Table 1
Fuel properties.

Property	Diesel	Syngas
Lower Heating Value, LHV (KJ/kg)	42600	43860
Density at 15°C (kg/m^3)	850	0.671
Stoichiometric fuel-air ratio	0.070	0.068

Table 2
Flame fuel combinations.

Liquid/gas fuel proportion (based on energy share)	Flow rates			Bulk swirling gas velocity (cm/s)
	Diesel (g/s)	Syngas (l/min)	Air (l/min)	
100/0	0.35	0.0	352	365
90/10	0.32	3.1	352	368
80/20	0.28	6.1	352	371
70/30	0.25	9.2	352	374

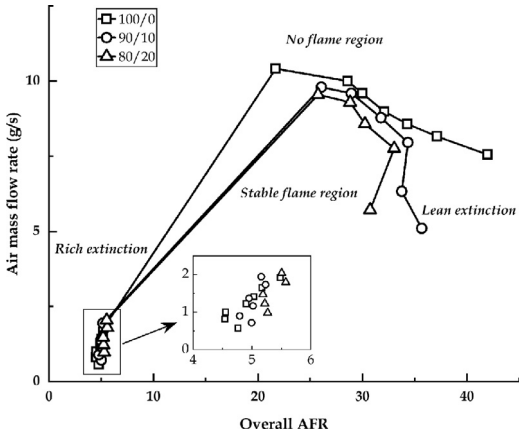

Fig. 2. Limits of stable flame operation.

The operating conditions for the optical and pollutant emissions tests were a constant power output of 15 kW and a global equivalence ratio of 0.7. As earlier mentioned, the total heat output is the sum of the heat contribution of each fuel based on the LHV of the fuels and the flow rate according to Eq. (2) where $\dot{m}$ represents the mass flow rate of fuel and the subscripts l and g stand for liquid and gas respectively. With the same denotations as in Eq. (2) and with φ_{global} referring to global equivalence ratio, the relevant combustion air mass flow rate is given by Eq. (3).

$$THO = (LHV_l \times \dot{m}_l) + (LHV_g \times \dot{m}_g) \tag{2}$$

$$\dot{m}_{air} = \frac{\dot{m}_g \times AFR_{Stoic,g} + \dot{m}_l \times AFR_{Stoic,l}}{\varphi_{global}} \tag{3}$$

The method utilised to define the stability limits in Section 3.1 is based on Lefebvre and Ballal [37] and involved carrying out a series of flame extinction tests at different heat outputs and noting the lean and rich extinction points. At each heat output, for the respective fuel combinations, a stable flame was established then the air flow rate was gradually increased until flame extinction occurred – the lean stability limit. The corresponding rich limit was determined by re-establishing the flame at the same heat output and then gradually decreasing the air flow rate until flame extinction occurred. These limits are presented in Section 3.1 for the neat diesel case and two blends of diesel/syngas. The power outputs used in the flame stability range study were 6 – 18 kW in steps of 2 kW for the 100/0 case; 8 – 18 kW in steps of 2 kW for the 90/10 case; and 10 – 18 kW in steps of 2 kW for the 80/20 case. The reduction of liquid flow rates as LGR decreases made it impractical to test, for instance, the 80/20 case at 6 and 8 kW. The reason being that, in the manner utilised, the employed pressure type nozzle is known to experience considerable variation in spray atomisation quality as liquid flow rates change [38].

2.4. Chemical kinetics modelling

To numerically explore diesel/syngas co-combustion in gas turbines, the reduced chemical kinetics mechanism created by Lawrence Livermore National Laboratory [39] was utilised in CHEMKIN-PRO for adiabatic flame temperature, laminar flame speed, heat release rate and pollutant emissions estimation [40]. Fuel combinations and operating conditions were set as in the experimental campaign with solutions based on an adaptive grid of 1000 points. The reaction mechanism comprised 323 chemical species with n-C_7H_{16} selected as diesel surrogate. However, the mechanism did not account for NO_X emissions and therefore was modified to predict NO_X emissions by adding the Zeldovich's reactions for NO_X formation to the reduced

Table 3
NO_X forming reactions [39].

Reactions	A	n	E_a
$N + NO = N_2 + O$	3.50E13	0.00	3.30E2
$N + O_2 = NO + O$	2.65E12	0.00	6.40E3
$N + OH = NO + H$	7.33E13	0.00	1.12E3
$N_2O + O = N_2 + O_2$	1.40E12	0.00	1.08E4
$N_2O + O = 2NO$	2.90E13	0.00	2.32E4
$N_2O + H = N_2 + OH$	4.40E14	0.00	1.89E4
$N_2O + OH = N_2 + HO_2$	2.00E12	0.00	2.11E4
$N_2O(+ M) = N_2 + O(+ M)$	1.30E11	0.00	5.96E4
$HO_2 + NO = NO_2 + OH$	2.11E12	0.00	-4.80E2
$NO + O + M = NO_2 + M$	1.06E20	-1.41	0.00E0
$NO_2 + O = NO + O_2$	3.90E12	0.00	-2.40E2
$NO_2 + H = NO + OH$	1.32E14	0.00	3.60E2

mechanism. As shown in Table 3, and similar to Feng [41], 12 additional reactions involving 4 elements were added to the mechanism with the first 4 reactions being the most significant.

The reaction rate k was calculated according to Eq. (4) in which A is the pre-exponential factor; T, the temperature in Kelvin; n, the temperature exponent of the ith reaction; E_a, the reaction activation energy and R, the universal gas constant.

$$k = AT^n e^{(-E_a/RT)} \tag{4}$$

3. Results and discussion

3.1. Limits of stable operation

In Fig. 2, the limits of stable flame operation for two different diesel/syngas blends – 90/10 and 80/20 – are presented alongside the stability limits of neat diesel flame in the same burner. Under test conditions, the region of stable burning for the different test conditions – the area under each curve of Fig. 2 – reduces as LGR decreases from 100/0 to 80/20 particularly in the fuel-lean section. The increasing momentum of the swirling stream of air/syngas as air flow rate is increased eventually causes the rate at which diesel spray particles are being swept away from the combustion zone to exceed the rate of recirculation of hot combustion products necessary to sustain the flame. As LGR decreases, this occurs sooner as the comparatively larger diesel spray particles require longer evaporation timescales and hence the hot combustion products are not as rapidly formed as in the finer spray of the 100/0 case.

While the aforementioned variation in spray quality might be a dominating factor, alteration in reacting flow dynamics as syngas is introduced into the diesel spray may also be contributing. Although it represents a single equivalence ratio, the distribution of the intermediate combustion species, C_2^* and CH*, in Fig. 3, suggests that with syngas present, combustion reactions commence and end faster with greater reactivity away from the burner centreline and more towards the edges of the burner. With that being the case, the diesel spray that is initially concentrated within a 60° cone angle around the burner centreline would have to quickly diffuse from the centre in order to participate in the reaction. The finer spray particles in the 100/0 case would be superior in this regard compared with the 90/10 and 80/20 cases.

Consequently, the range of stable flame operation as defined in Fig. 2 gets narrower as the liquid fraction of fuel mix decreases. The noted contraction in the range of air-fuel ratios over which stable flames exist as fuel LGR changes must not be misconstrued as being same for flame stability at a particular operating point. In fact, as shown later, diesel flame stability improves when co-combusted with 20% or 30% syngas. Nevertheless, the reduction in stable flame operating range is undesirable for gas turbine combustors and, given the explanation offered, a different injection strategy for the liquid fuel that does not significantly alter atomisation quality as flow rates change like the air blast nozzle may yield improved results.

3.2. Optical emissions

A false colormap representation of the distribution of C_2^* and CH* species in diesel and diesel/syngas flames at 15 kW and equivalence ratio (ER) of 0.7 is shown in Fig. 3. The images are normalised to the highest intensity for each species across the entire range of fuel blends shown. Although both sets of chemiluminescence images appear similar, their known formation pathways are different. From [35] the main formation reactions for the intermediate species CH* are $C_2H + O_2 \rightarrow CO_2 + CH^*$ and $C_2H + O \rightarrow CO + CH^*$ whereas that of C_2^* is $CH_2 + C \rightarrow C_2^* + H_2$. Also, as will be discussed later, the chemiluminescence intensity levels of both species are different.

Whereas both species have a U-shaped distribution about the centreline of the burner for the 100/0 case; in the multiphase cases, the distribution of C_2^* and CH* species assume more of a V-shape with the species spreading further away from the burner centreline towards the edges and all but separating in the middle for the 80/20 and 70/30 cases. A possible explanation for this, and supported by [42,43], is that the central recirculation zone is weakened while the outer recirculation zone is strengthened as the local equivalence ratio of the of the swirling flow increases with a rise in gas fraction in fuel mix.

Also, it appears that in the multiphase combustion cases, the reaction zone is closer to the nozzle orifice plane compared to 100/0 case. Thus introduction of syngas into the burning diesel spray causes a quicker onset of C_2^*/CH*-forming reactions as higher concentrations of these species are evident well before the 20 mm axial position in the multiphase cases compared to the 100/0 case. Moreover, the reactions forming the intermediate combustion species, appear not only to start sooner but also to end quicker in the multiphase cases in relation to the 100/0 case as evident in the axial distribution of the species in Fig. 3. This assertion is corroborated by the flame speed trend in Fig. 4(a) obtained from chemical kinetics analysis. One implication of this – higher flame speed hence shorter residence time – for diesel/syngas fuel burn compared to neat diesel burn is that relatively lesser time is available for liquid fuel evaporation and subsequent combustion. Bear in mind that the lower liquid flow rate at 70/30, for instance, is expected to have poorer spray quality than the flowrate at 100/0 given the atomiser operating strategy employed thereby requiring a longer evaporation timescale. Consequently, the volumetric heat release rate decreases as gas content of fuel mix increases as shown by chemical kinetics analysis (Fig 4b) as does the adiabatic flame temperature (Fig. 4c). C_2^* and CH* species chemiluminescence are reasonably good indicators of heat release rate and the intensity variation of these species from Fig. 3 appear to generally support the trend of Fig. 4(b).

Further, assuming that the heat release rate at a particular instance is a function of the integral intensity (II) of either the C_2^* or CH* radicals at that instance, the temporal variation of the rate of heat release from the flames were determined. This approach is similar to that in Ballester et al. [44] and as samples, the variation of C_2^* species integral intensity across the duration of the 250 captured images is shown for the 100/0 case in Fig. 5(a) and for the 70/30 case in Fig. 5(b).

The corresponding CH* species integral intensity is shown in Fig. 5 (c) and Fig. 5(d). The thick solid horizontal line represents the average integral intensity of the 250 images. As this average value varies across fuel blends, a simple standard deviation of each data set is inadequate to enable comparison of the temporal variability of heat release rate across the tested fuel compositions. Instead, the coefficient of variation, the ratio of the standard deviation of each data set to the corresponding mean value has been utilised as shown in Fig. 6. Interestingly, apart from the 90/10 case with the greatest variability

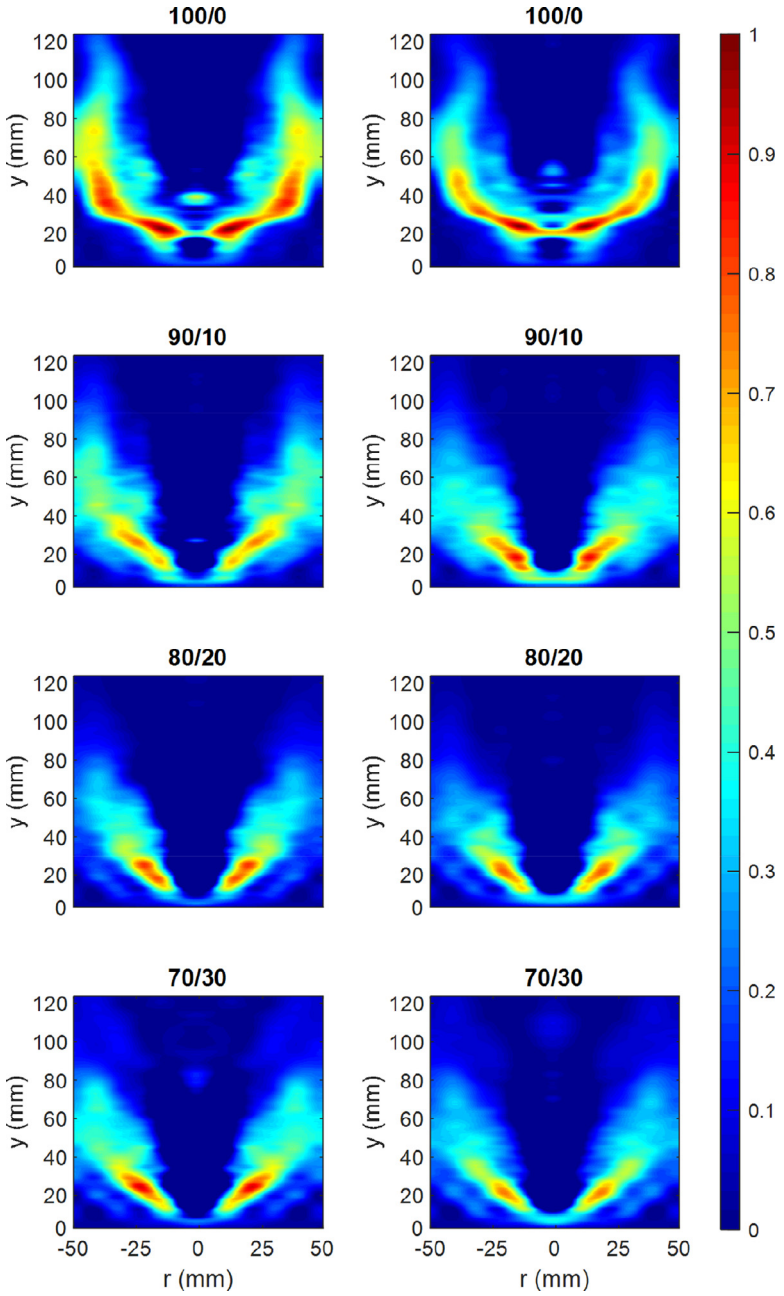

Fig. 3. Abel deconvoluted images of C_2^* (left column) and CH^* (right column) species normalised to the highest intensity in each category. Flow is from bottom to top.

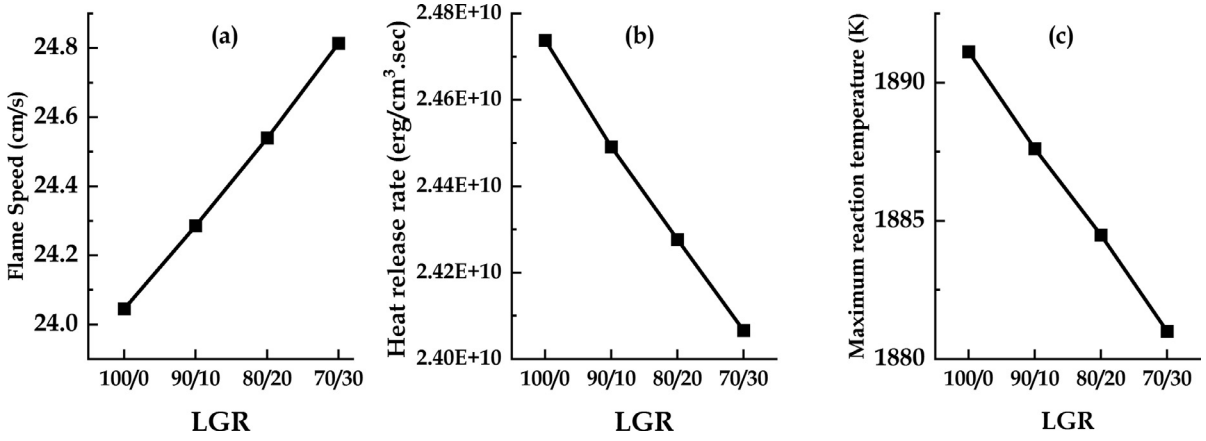

Fig. 4. Diesel/syngas (a) flame speed (b) volumetric heat release rate and (c) maximum flame temperature from chemical kinetics analysis.

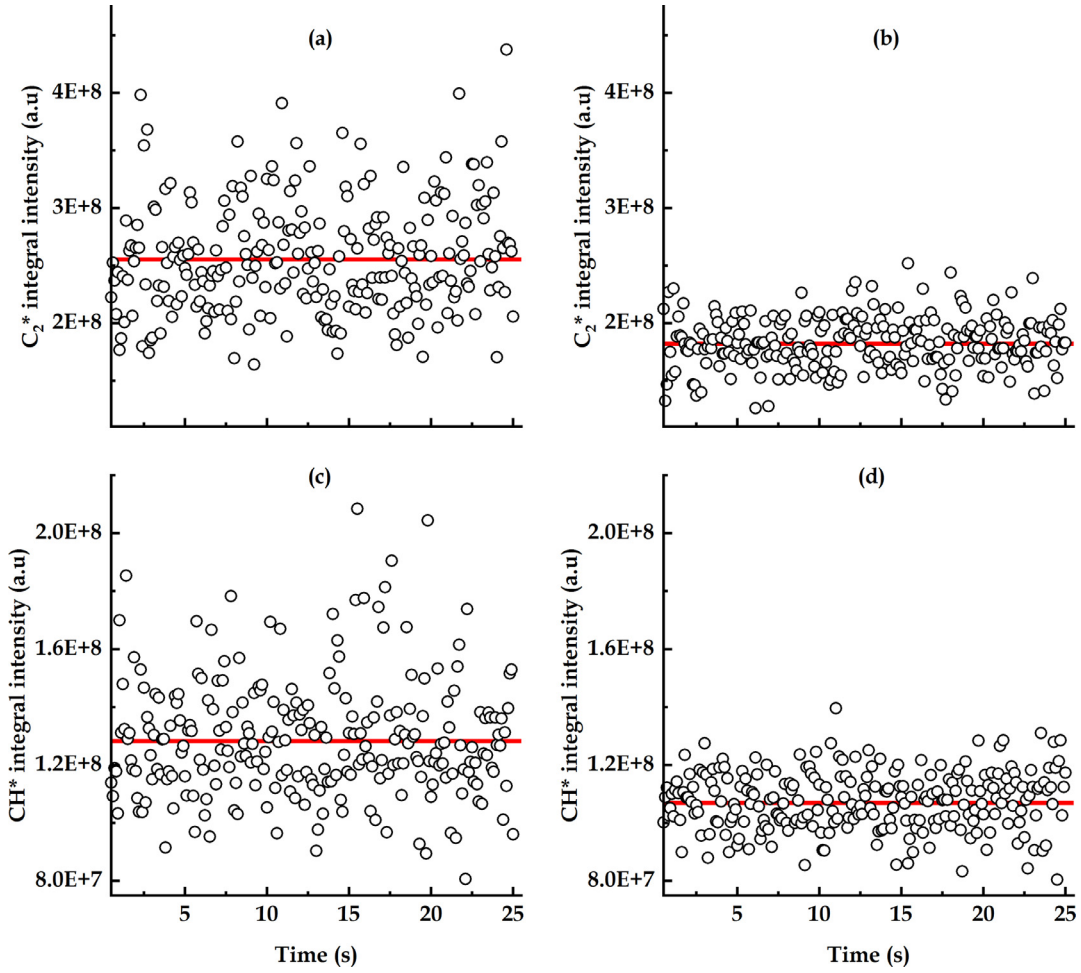

Fig. 5. Temporal variation of C_2^* species integral intensity for (a) 100/0 (b) 70/30 and CH* species integral intensity for (c) 100/0 (d) 70/30 diesel/syngas flames.

in heat release rate across all the test cases, diesel/syngas combustion of up to 70/30 combination by energy share ratio, results in lesser fluctuation in the rate of heat release compared with neat diesel fuel combustion. Lesser fluctuation in heat release rate promotes a more stable flame and potentially reduces combustion noise. From Fig. 6, then, a 70/30 combination of diesel/syngas that delivers the same power output as 100% diesel combustion demonstrates about 7% better performance in terms of flame stability.

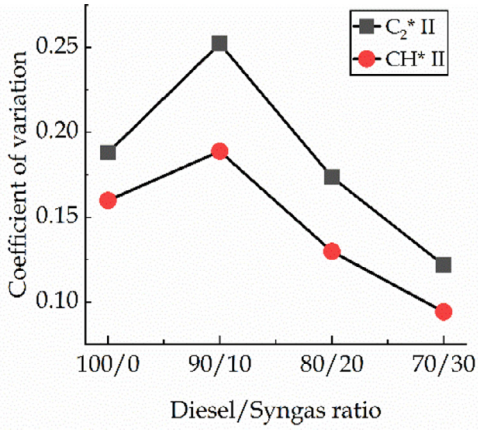

Fig. 6. Comparison of the temporal variability of heat release rate across tested fuel compositions.

3.3. Post combustion emissions

The flue gas emissions of CO and NO_X from the experimental tests are presented in Fig. 7 and Fig. 8 respectively. Each is accompanied by the chemical kinetics estimation of each pollutant presented in emissions index (EI) form. The chemical kinetics simulation results are shown not for value comparison but to demonstrate the fairly similar trend with experimental results suggesting that changing reacting flow chemistry contributes to the emissions variation. From Fig 7, increase in CO emissions is recorded as gas ratio of fuel composition increases. From experimental data, there is a 48% increase in CO emissions as fuels change from 100/0 diesel/syngas to 90/10 and by a further 50% from 90/10 to 80/20. Thereafter, there is a 66% increment in CO emissions from the 80/20 case to the 70/30 case. The gradual and then rapid rise in CO emissions as diesel fuel fraction decreases is attributable to several inter-related factors.

First, as mentioned previously, the reduction in diesel flow rate as LGR is altered while maintaining pressure drop upstream of the MFC results in poorer liquid fuel atomisation. Poor liquid fuel atomisation results in relatively larger droplets which require comparatively more time for evaporation and combustion. The flame speed trend shown in Fig. 4(a) implies a decreasing flame residence time as LGR decreases, further adding to the adverse effect of poorer atomisation. Additionally, the alteration in reacting flow dynamics earlier discussed (section 3.2), exacerbates the CO problem as syngas partly replaces diesel in the fuel mix. Second, the heat release rate trend of Fig. 4(b), supported by the intermediate combustion species intensity variation in Fig. 3, suggests a reduction in adiabatic flame temperature as diesel/syngas ratio changes

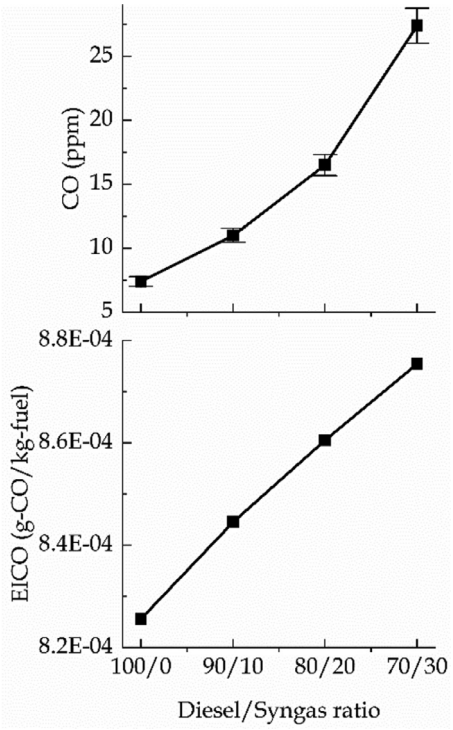

Fig. 7. CO emissions from diesel/syngas flames (top) experimental (bottom) CHEMKIN analysis.

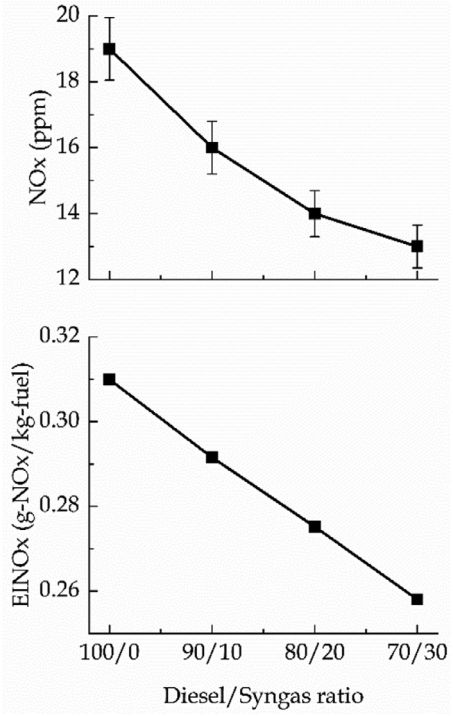

Fig. 8. NO_X emissions from diesel/syngas flames (top) experimental (bottom) CHEMKIN analysis.

from 100/0 to 70/30. The chemical analysis simulation proves this as shown in Fig. 4(c). The decreasing flame temperatures observed as syngas ratio in fuel blend increases contributes to the noted variation in CO emissions.

The conditions elaborated in the foregoing that prove unfavourable for CO oxidation, serve to lower NO_X emissions. Lower adiabatic flame temperature arising from reduction in heat release rate together with shorter residence times occasioned by higher flame speeds as gas ratio in fuel blend increases causes a steady reduction in NO_X emissions as shown in Fig. 8.

Conclusions

Three blends of diesel and syngas were combusted in a model swirl-stabilised gas turbine combustor to experimentally study multiphase fuel burn in continuous flow engines. The utilised syngas – a 10% by volume mixture of each of CO and H_2 with the balance being CH_4 – was introduced into the combustion air upstream of the burning diesel spray. Range of stable flame operation, flame stability and post combustion emissions comparisons were made between the neat diesel combustion and the diesel/syngas co-combustion cases. Apart from the instance of determining the stable operating range, the diesel/syngas and air combination was selected to deliver a power output of 15 kW at a global equivalence ratio of 0.7. Also, a numerical study was conducted using the syngas composition as in the experiment and n-C_7H_{16} as a diesel surrogate in CHEMKIN-PRO to establish trends in flame speed, heat release rate and adiabatic flame temperature. The main findings from the study were:

1. Co-combusting diesel and syngas in a swirl-stabilised gas turbine combustor using the fuel injection procedure described in this work reduces the achievable range of stable flame operation compared with neat diesel combustion.
2. At the chosen operating point – 15 kW overall heat output at a global equivalence ratio of 0.7 – flame stability, determined by the extent of the temporal fluctuation of C_2^* and CH^* species chemiluminescence, improves by 7% when diesel flow rate is reduced to allow 30% of the overall heat output to be supplied by syngas. However, heat release rate is sacrificed as suggested by chemical kinetics analysis as well the observed intensity variation of the aforementioned intermediate combustion species.
3. NO_X emissions are steadily reduced whereas CO emissions are increased as syngas partly replaces diesel in the combustion process. While the emissions trend is mainly attributed to the loss in spray quality from the pressure atomiser as diesel flow rates change, the alteration in reacting flow chemistry as fuel composition changes might be contributing as indicated by the chemical kinetics simulation.

Declaration of Competing Interest

The authors declare that they have no known competing financial interests or personal relationships that could have appeared to influence the work reported in this paper.

Acknowledgement

We are grateful to Mr. Malcolm Seaborne and Ms. Amie Parnell for their help in construction and installation of the dual fuel burner. Ogbonnaya Agwu is grateful to the Petroleum Technology Development Fund (PTDF) for sponsoring his PhD studies at Cardiff University. Dr. A. Valera-Medina gratefully acknowledges the support from the Welsh European Funding Office (WEFO) through its program "Flexible Integrated Energy Systems (FLEXIS)". Project No. 80835.

References

[1] M.J. Abedin, A. Imran, H.H. Masjuki, M.A. Kalam, S.A. Shahir, M. Varman, A.M. Ruhul, An overview on comparative engine performance and emission characteristics of different techniques involved in diesel engine as dual-fuel engine operation, Renew. Sust. Energy Rev. 60 (2016) 306–316.

[2] K. Cheenkachorn, C. Poompipatpong, C.G. Ho, Performance and emissions of a heavy-duty diesel engine fuelled with diesel and LNG (liquid natural gas), Energy 53 (2013) 52–57.
[3] L. Wei, P. Geng, A review on natural gas/diesel dual fuel combustion, emissions and performance, Fuel Process. Technol. 142 (2016) 264–278.
[4] R.G. Papagiannakis, D.T. Hountalas, Experimental investigation concerning the effect of natural gas percentage on performance and emissions of a DI dual fuel diesel engine, Appl. Therm. Eng. 23 (2003) 353–365.
[5] R.G. Papagiannakis, C.D. Rakopoulos, D.T. Hountalas, D.C. Rakopoulos, Emission characteristics of high speed, dual fuel, compression ignition engine operating in a wide range of natural gas/diesel fuel proportions, Fuel 89 (2010) 1397–1406.
[6] P. Dimitriou, M. Kumar, T. Tsujimura, Y. Suzuki, Combustion and emission characteristics of a hydrogen-diesel dual fuel engine, Int. J. Hydrogen Energy 43 (2018) 13605–13617.
[7] P. Dimitriou, T. Tsujimura, T. Suzuki, Hydrogen-diesel dual-fuel engine optimization for CHP systems, Energy 160 (2018) 740–752.
[8] A. Sarkar, U.K. Saha, Role of global fuel-air equivalence ratio and preheating on the behaviour of a biogas driven dual fuel diesel engine, Fuel 232 (2018) 743–754.
[9] C.C.M. Luijten, E. Kerkhof, Jatropha oil and biogas in a dual fuel CI engine for rural electrification, Energy Convers. Manag. 52 (2011) 1426–1438.
[10] Z. Chen, L. Wang, K. Zeng, A comparative study on the combustion and emissions of dual-fuel engine fueled with natural gas/methanol, natural gas/ethanol, and natural gas/nbutanol, Energy Convers. Manag. 192 (2019) 11–19.
[11] M. Buffi, A. Cappelletti, A.M. Rizzo, F. Martelli, D. Chiaramonti, Combustion of fast pyrolysis bio-oil and blends in a micro gas turbine, Biomass Bioenergy 115 (2018) 174–185.
[12] M. Buffi, A. Valera-Medina, R. Marsh, D. Pugh, A. Giles, J. Runyon, D. Chiaramonti, Emissions characterization tests for hydrotreated renewable jet fuel from used cooking oil and its blends, Appl. Energy 201 (2017) 84–93.
[13] H. Kurji, A. Valera-Medina, J. Runyon, A. Giles, D. Pugh, R. Marsh, N. Cerone, F. Zimbardi, V. Valerio, Combustion characteristics of biodiesel saturated with pyrolysis oil for power generation in gas turbines, Renew. Energy 99 (2016) 443–451.
[14] C.T. Chong, S. Hochgreb, Flame structure, spectroscopy and emissions quantification of rapeseed biodiesel under model gas turbine conditions, Appl. Energy 185 (2017) 1383–1392.
[15] H.V. Panchasara, B.M. Simmons, A.K. Agrawal, A.K. Spear, D.T. Daly, Combustion performance of biodiesel and diesel-vegetable oil blends in a simulated gas turbine burner, J. Eng. Gas Turbine. Power 131 (2009) 031503-1-11.
[16] H. Xiao, A. Valera-Medina, P.J. Bowen, Study on premixed combustion characteristics of co-firing ammonia/methane fuels, Energy 140 (2017) 125–135.
[17] H. Xiao, A. Valera-Medina, R. Marsh, P.J. Bowen, Numerical study assessing various ammonia/methane reaction models for use under gas turbine conditions, Fuel 196 (2017) 344–351.
[18] H. Xiao, A. Valera-Medina, Chemical kinetic mechanism study on premixed combustion of ammonia/hydrogen fuels for gas turbine use, J. Eng. Gas Turbine. Power 131 (2009) 081504-1-10.
[19] M.C. Lee, S.B. Seo, J.H. Chung, S.M. Kim, Y.J. Joo, D.H. Ahn, Gas turbine combustion performance test of hydrogen and carbon monoxide synthetic gas, Fuel 89 (2010) 1485–1491.
[20] M.C. Lee, A.B. Seo, J. Yoon, M. Kim, Y. Yoon, Experimental study on the effect of N_2, CO_2, and steam dilution on the combustion performance of H_2 and CO synthetic gas in an industrial gas turbine, Fuel 102 (2012) 431–438.
[21] A. Valera-Medina, D.G. Pugh, P. Marsh, G. Bulat, P. Bowen, Preliminary study on lean premixed combustion of ammonia-hydrogen for swirling gas turbine combustors, Int. J. Hydrogen Energy 42 (2017) 24495–24503.
[22] A. Valera-Medina, P. Marsh, J. Runyon, D.G. Pugh, P. Beasley, T. Hughes, P. Bowen, Ammonia-methane combustion in tangential swirl burners for gas turbine power generation, Appl. Energy 185 (2017) 1362–1371.
[23] J. Sidey, E. Mastorakos, Visualisation of turbulent swirling dual-fuel flames, Proc. Combust. Inst. 36 (2017) 1721–1727.
[24] J.A.M. Sidey, E. Mastorakos, Stabilisation of swirling dual-fuel flames, Exp. Therm. Fluid Sci. 95 (2018) 65–72.
[25] M.J. Evans, J.A.M. Sidey, J. Ye, P.R. Medwell, B.B. Dally, E. Mastorakos, Temperature and reaction zone imaging in turbulent swirling dual-fuel flames, Proc. Combust. Inst. 37 (2019) 2159–2166.
[26] Altaher, M.A., Li, H., Andrews, G.Co-firing of kerosene and biodiesel with natural gas in a low NOx radial swirl combustor. In Proceedings of ASME Turbo Expo 2012 (GT2012-68597): Copenhagen, Denmark. https://doi.org/10.1115/GT2012-68597.
[27] C.T. Chong, M. Chiong, J. Ng, M. Tran, A. Valera-Medina, V. Jozsa, B. Tian, Dual-fuel operation of biodiesel and natural gas in a model gas turbine combustor, Energy Fuels (2020) https://doi.org/10.1021/acs.energyfuels.9b04371 .
[28] F. Delattin, G. Di Lorenzo, S. Rizzo, S. Bram, J. De Ruyck, Combustion of syngas in a pressurized microturbine-like combustor: experimental results, Appl. Energy 87 (2010) 1441–1452.
[29] H.J. Kurji, Fuel Flexibility with low emissions for gas turbine engines. PhD Thesis. Cardiff University, Cardiff, UK, 2017.
[30] K. Liu, J.P. Wood, E.R. Buchanan, P. Martin, V.E. Sanderson, Biodiesel as an alternative fuel in siemens dry low emissions combustors: atmospheric and high pressure rig testing, J. Eng. Gas Turbine. Power 132 (2010) 011501-1-9.
[31] C.T. Chong, S. Hochgreb, Flame structure, spectroscopy and emissions quantification of rapeseed biodiesel under model gas turbine conditions, Appl. Energy 185 (2017) 1383–1392.
[32] T. Kathrotia, U. Riedel, A. Siepel, K. Moshammer, A. Brockhinke, Experimental and numerical study of chemiluminescent species in low-pressure flames, Appl. Phys. B 107 (2012) 571–584.
[33] T. Garcia-Armingol, Y. Hardalupas, A.M.K.P. Taylor, J. Ballester, Effect of local flame properties on chemiluminescence-based stoichiometry measurement, Exp. Therm. Fluid Sci. 53 (2014) 93–103.
[34] Morell M.R., Seitzman J., Wilensky M., Lubarsky E., Lee J., Zinn B.Interpretation of Optical Emissions for Sensors in Liquid Fuelled Combustors. 39th Aerospace Sciences Meeting and Exhibit, Reno, NV, USA. AIAA-2001-0787.
[35] J. Ballester, T. Garcia-Armingol, Diagnostic techniques for the monitoring and control of practical flames, Prog. Energy Combust. Sci 36 (2010) 375–411.
[36] J. Runyon, R. Marsh, P. Bowen, D. Pugh, A. Giles, S. Morris, Lean methane flame stability in a premixed generic swirl burner: isothermal flow and atmospheric combustion characterization, Exp. Therm. Fluid Sci. 92 (2018) 125–140.
[37] Lefebvre A.H., Ballal D.R.Gas Turbine Combustion Alternative Fuels and Emissions, 3rd ed., CRC Press Taylor & Francis Group, 2010, p. 168.
[38] N. Hashimoto, Y. Ozawa, N. Mori, I. Yuri, T. Hisamatsu, Fundamental combustion characteristics of palm methyl ester (PME) as alternative fuel for gas turbines, Fuel 87 (2008) 3373–3378.
[39] M. Mehl, W.J. Pitz, C.K. Westbrook, H.J. Curran, Kinetic modeling of gasoline surrogate components and mixtures under engine conditions, Proc. Combust. Inst. 33 (2011) 193–200.
[40] Reaction Design, CHEMKIN-PRO 15092. San Diego, California, 2009.
[41] S. Feng, Numerical study of the performance and emission of a diesel-syngas dual fuel engine, Math. Problems Eng. (2017) Article ID 6825079 https://doi.org/10.1155/2017/6825079 .
[42] A. Valera-Medina, N. Syred, P. Bowen, Central recirculation zone visualization in confined swirl combustors for terrestrial energy, J. Propul. Power 29 (1) (2013), doi: 10.2514/1.B34600.
[43] N. Syred, A review of oscillation mechanisms and the role of the precessing vortex core (PVC) in swirl combustion systems, Prog. Energy Combust. Sci 32 (2006) 93–161.
[44] J. Ballester, R. Hernandez, A. Sanz, A. Smolarz, J. Barroso, A. Pina, Chemiluminescence monitoring in premixed flames of natural gas and its blends with hydrogen, Proc. Combust. Inst. 32 (2009) 2983–2991.